Chemistry & Biology
Article

Crystal Structures of Sirt3 Complexes with 4′-Bromo-Resveratrol Reveal Binding Sites and Inhibition Mechanism

Giang Thi Tuyet Nguyen,[1,2] Melanie Gertz,[1,2] and Clemens Steegborn[1,*]
[1]Department of Biochemistry, University of Bayreuth, 95440 Bayreuth, Germany
[2]These authors contributed equally to this work
*Correspondence: clemens.steegborn@uni-bayreuth.de
http://dx.doi.org/10.1016/j.chembiol.2013.09.019

SUMMARY

Sirtuins are protein deacetylases regulating aging processes and various physiological functions. Resveratrol, a polyphenol found in red wine, activates human Sirt1 and inhibits Sirt3, and it can mimic calorie restriction effects, such as lifespan extension in lower organisms. The mechanism of Sirtuin modulation by resveratrol is not well understood. We used 4′-bromo-resveratrol (5-(2-(4-hydroxyphenyl)vinyl)-1,3-benzenediol) to study Sirt1 and Sirt3 modulation. Despite its similarity to the Sirt1 activator resveratrol, the compound potently inhibited both, Sirt1 and Sirt3. Crystal structures of Sirt3 in complex with a fluorophore-labeled and with a native substrate peptide, respectively, in presence of 4′-bromo-resveratrol reveal two compound binding sites. Biochemical studies identify the internal site and substrate competition as the mechanism for inhibition, providing a drug target site, and homology modeling suggests that the second, allosteric site might indicate the site for Sirt1 activation.

INTRODUCTION

Sirtuins are NAD^+-dependent protein deacetylases conserved throughout evolution. They deacetylate various targets and thereby control cellular processes ranging from genomic integrity to stress responses and metabolism (Haigis and Sinclair, 2010; Michan and Sinclair, 2007). In mammals, there are seven Sirtuin isoforms, Sirt1–7, that differ in their cellular localization and function (Haigis and Sinclair, 2010; Michan and Sinclair, 2007). The nuclear Sirtuins Sirt1, 6, and 7 deacetylate proteins contributing to DNA maintenance and transcription such as Ku70 and p53 (Haigis and Sinclair, 2010). The mainly cytosolic Sirt2 regulates, for example, tubulin polymerization (North et al., 2003). Among the mitochondrial isoforms Sirt3, 4, and 5, Sirt3 appears to be the major deacetylase and a key regulator of metabolism especially for adaption to limited nutrient supply (Newman et al., 2012). Consistently, Sirt3 regulates substrates involved, for example, in ATP production, fatty acid oxidation, and the citric acid cycle but also in mitochondrial integrity, oxidative stress responses, and apoptosis (Hebert et al., 2013; Verdin et al., 2010). Sirt4 influences fatty acid metabolism through deacetylation of malonyl-CoA decarboxylase (Laurent et al., 2013), and strong evidence links this isoform to insulin secretion (Haigis et al., 2006). Sirt5 was recently described to more efficiently demalonylate or desuccinylate its substrates (Du et al., 2011) and it was reported to regulate the urea cycle through its target carbamoyl phosphate synthetase 1 (CPS1; Gertz and Steegborn, 2010; Nakagawa et al., 2009).

Sirtuins share a highly conserved catalytic core but differ in N- and C-terminal extensions (Frye, 2000; Sanders et al., 2010). The catalytic core consists of two domains (Sanders et al., 2010; Sauve et al., 2006), a larger Rossmann-fold domain typical for NAD^+ binding proteins and a smaller, more variable zinc-binding domain. The zinc ion is coordinated by four invariant cysteines and appears essential for the stability of the protein (Sauve et al., 2006). The acetylated substrate and the NAD^+ cosubstrate bind in a cleft between the two domains thereby inducing closure of the active site (Jin et al., 2009) and stabilization of a so-called cofactor binding loop (Sanders et al., 2010). In a productive conformation, the nicotinamide moiety of NAD^+ is buried in the highly conserved C pocket (Hoff et al., 2006). Thereby, the glycosidic bond to the nicotinamide ribose is stretched, which facilitates nicotinamide release and alkylamide formation between acetyl-Lys and the ADP-ribose 1′-C position (Sauve and Youn, 2012). Hydrolysis of the alkylimidate leads to the products, deacetylated protein and 2′-O-acetyl-ADP-ribose (OAADPr) (Sauve and Youn, 2012).

Sirtuins contribute to the regulation of aging processes and aging-related diseases, such as neurological disorders or metabolic syndrome (Rahman and Islam, 2011), and they were shown to mediate lifespan-extending effects of caloric restriction (CR; Cohen et al., 2004; Guarente, 2005; Guarente and Picard, 2005). Thus, they are considered attractive drug targets. Extensive efforts to develop Sirtuin inhibitors and activators (Chen, 2011; Villalba and Alcaín, 2012), however, yielded few promising compounds, such as the potent and mildly Sirt1-specific inhibitor Ex-527 (Napper et al., 2005). Most other Sirtuin modulators suffer from low potency and/or specificity, and mechanistic investigations are needed for their improvement. The polyphenol resveratrol (3,5,4′-trihydroxy-*trans*-stilbene; Figure 1A) was shown to activate Sirt1 and to induce Sirtuin mediated lifespan-extension similar to CR (Howitz et al., 2003). However, resveratrol shows low potency against Sirt1 and affects several cellular targets (Park et al., 2012; Pirola and Fröjdö, 2008). In

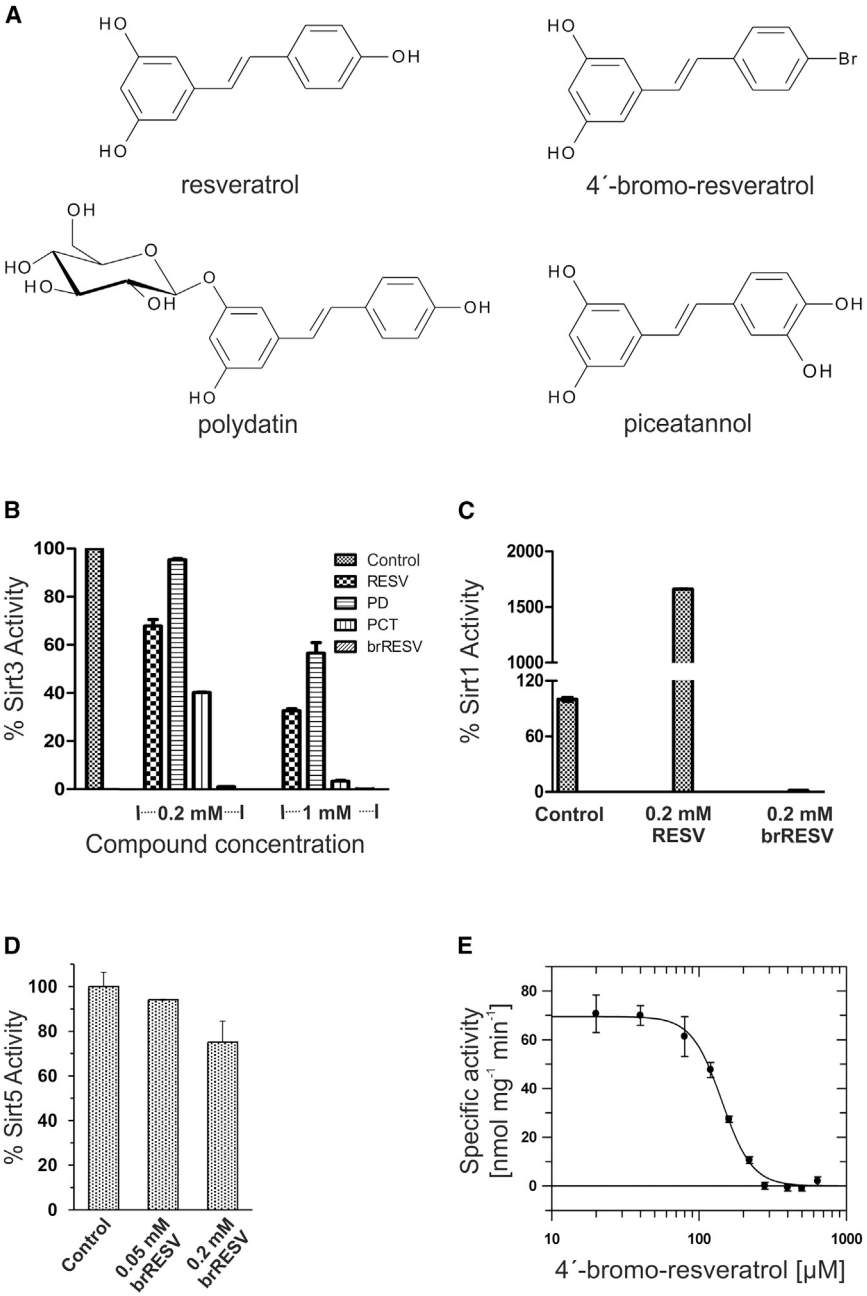

Figure 1. 4′-Bromo-Resveratrol Is a Potent hSirt3 Inhibitor

(A) Chemical structures of resveratrol (3,5,4′-trihydroxy-*trans*-stilbene) and its related compounds 4′-bromo-resveratrol (5-(2-(4-hydroxyphenyl)vinyl)-1,3-benzenediol), polydatin (reservatrol-3-β-D-glucoside), and piceatannol (3,5,3′,4′-tetrahydroxy-*trans*-stilbene).

(B) Inhibition of hSirt3 by resveratrol-related compounds in the FdL assay at 0.2 mM and 1 mM compound concentrations. Activities are normalized to the control in the absence of compounds. Error bars: SD from two independent measurements. RESV, resveratrol; brRESV, 40-bromoresveratrol; PCT, piceatannol; PD, polydatin.

(C) Resveratrol (0.2 mM) activates hSirt1 in the FdL assay, whereas 4′-bromo-resveratrol inhibits. Activities were normalized to the control in absence of compound. Error bars: SD from two independent measurements.

(D) Up to 0.2 mM 4′-bromo-resveratrol inhibit the Sirt5 desuccinylase activity against succinylated FdL substrate only weakly. Activities were normalized to the control in absence of compound. Error bars: SD from two independent measurements.

(E) IC_{50} determination of 4′-bromo-resveratrol on hSirt3 against 500 μM ACS2 peptide using MS. Error bars: SE of linear fits to time series experiments.

fact, we recently showed that resveratrol can also activate Sirt5 and inhibit Sirt3 (Gertz et al., 2012). Crystal structures revealed that the modulating effect of resveratrol and its analog piceatannol (3,5,3′,4′-tetrahydroxy-*trans*-stilbene; Figure 1A) is based on a direct interaction with the substrate in case of the fluorophor-labeled Fluor-de-Lys (FdL) peptide used in that study.

We used 4′-bromo-resveratrol (5-(2-(4-hydroxyphenyl)vinyl)-1,3-benzenediol; Figure 1A) as a tool for crystallographic studies with fluorophore-free substrate peptide. Interestingly, the bromo group dramatically increases the compound's potency on human Sirt3 (hSirt3) and it also inhibits, rather than activates, hSirt1. Crystal structures of hSirt3 in complex with peptide and 4′-bromo-resveratrol reveal two binding sites for this compound scaffold. Binding analyses and enzyme kinetics reveal inhibition site and mechanism, and our data further suggest a potential resveratrol binding site for hSirt1 activation.

RESULTS

4′-Bromo-Resveratrol Is a Potent hSirt3 Inhibitor

We previously found that the hSirt1 activator resveratrol also affects hSirt3 and hSirt5 activity (Gertz et al., 2012), but the compound shows a low potency against all Sirtuins. We therefore tested 4′-bromo-resveratrol effects on Sirtuins to identify a resveratrol derivative that shows higher solubility and can be unequivocally located in crystal structures based on the halogen's anomalous signal. Testing resveratrol and its analogs piceatannol, polydatin (reservatrol-3-β-D-glucoside), and 4′-bromo-resveratrol (Figure 1A) against hSirt3 in the FdL assay confirmed the weak inhibition by resveratrol and piceatannol (Gertz et al., 2012) and showed an even weaker effect for polydatin (Figure 1B). Surprisingly, 4′-bromo-resveratrol showed a much more potent effect and inhibited hSirt3 activity almost completely at 0.2 mM compound concentration (Figure 1B). Interestingly, we found the same, inhibitory effect of 0.2 mM 4′-bromo-resveratrol on hSirt1, in contrast to the ~17-fold activation by 0.2 mM resveratrol (Figure 1C). In contrast to its effect on Sirt1 and Sirt3, 4′-bromo-resveratrol

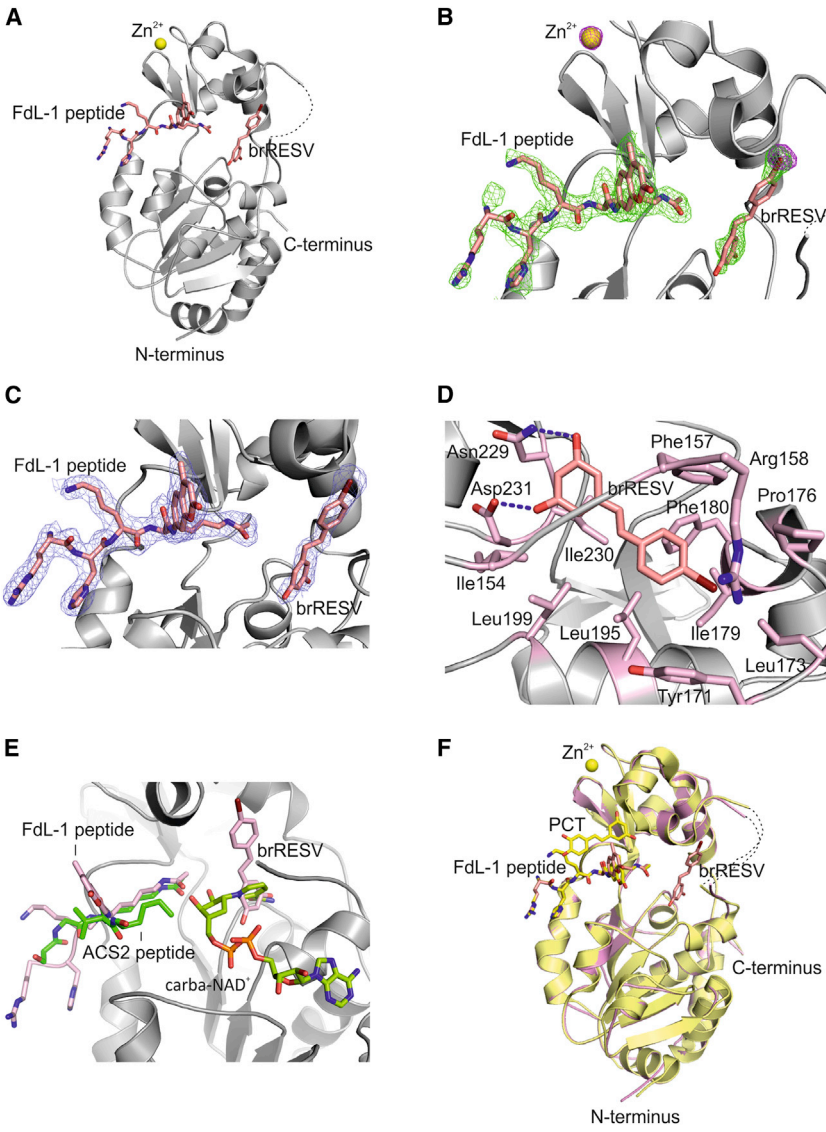

Figure 2. Crystal Structure of hSirt3 in Complex with 4′-Bromo-Resveratrol and FdL-1 Peptide

(A) Overall structure of hSirt3/FdL-1/4′-bromo-resveratrol complex. The dashed line indicates a loop not defined by electron density.

(B) FdL-1 peptide and 4′-bromo-resveratrol ligands of hSirt3, overlaid with omit F_o-F_c difference density (2.5σ; green) and anomalous density (5σ; magenta) showing the positions of Br and Zn^{2+}. See Figure S1 for anomalous density contoured at various σ levels.

(C) hSirt3/FdL-1/4′-bromo-resveratrol complex structure with $2F_o$-F_c density for the ligands contoured at 1σ.

(D) Closer view on the 4′-bromo-resveratrol binding site showing interacting residues. Hydrogen bonds are indicated by dashed lines.

(E) Superposition of the hSirt3/FdL-1/4′-bromo-resveratrol structure with a hSirt3/ACS2/carba-NAD^+ complex (PDB ID 4FVT; Szczepankiewicz et al., 2012). FdL-1 peptide and 4′-bromo-resveratrol are shown in pink, p53 peptide and NAD^+ in green. The protein part of the hSirt3/ACS2/carba-NAD^+ complex is omitted for clarity.

(F) Superposition of the hSirt3/FdL-1/4′-bromo-resveratrol (pink) with the hSirt3/FdL-1/PCT complex (yellow, PDB ID 4HD8; Gertz et al., 2012). FdL-1 peptide and 4′-bromo-resveratrol are shown in pink, FdL-1 peptide and PCT in yellow.

(A, B, and E) The missing loop is indicated by a dashed line. bRESV, 4′-bromo-resveratrol; PCT, piceatannol.

inhibited the desuccinylation activity of Sirt5 only weakly (Figure 1D). This partial selectivity and the increased potency against hSirt1 and hSirt3 suggest that this compound scaffold and its binding site bear potential for the development of isoform-selective Sirtuin inhibitors.

The FdL substrate peptide carries a fluorophor that can interact with small molecules, potentially leading to artificial effects on Sirtuin activity (Borra et al., 2004; Gertz et al., 2012; Pacholec et al., 2010). We therefore used a mass spectrometry (MS)-based assay and a fluorophore-free acetylated peptide derived from the physiological Sirt3 target acetyl-CoA synthetase 2 (ACS2) as a substrate to confirm and quantify hSirt3 inhibition by 4′-bromo-resveratrol. A dose-response experiment at 500 μM ACS2 peptide concentration yielded an half-maximal inhibitory concentration (IC_{50}) value of 143.0 ± 3.6 μM (Figure 1E). This result confirms that inhibition by 4′-bromo-resveratrol applies to fluorophore-free peptides and the lower potency in this assay, performed at higher peptide concentration, might indicate competition with this substrate (see also below).

Crystal Structure of hSirt3 in Complex with 4′-Bromo-Resveratrol and FdL-1 Peptide

To identify binding site and inhibition mechanism of 4′-bromo-resveratrol, we first co-crystallized hSirt3 and compound in the presence of FdL-1 peptide. In the resulting hSirt3/FdL-1/4′-bromo-resveratrol complex structure, the compound was found in the active site (Figures 2A–2C; Table 1). Significant F_o-F_c omit density (Figure 2B) indicated compound position and orientation, which was confirmed by a strong anomalous signal for the inhibitor's 4′-bromo atom (Figure 2B; Figure S1 available online), and complex refinement resulted in excellent $2F_o$-F_c density for the ligand (Figure 2C). Interestingly, the inhibitor is arranged differently from the weaker inhibitor piceatannol in the previously solved hSirt3/FdL-1/piceatannol complex (Gertz et al., 2012; see below). A closer look at the compound binding site (Figure 2D) shows that the A-ring hydroxyl groups of 4′-bromo-resveratrol form hydrogen bonds with Asn229 and Asp231 of hSirt3. Furthermore, residues Ile230, Leu199, and Ile154 form a hydrophobic patch for A-ring binding, and Phe157, Leu195, and Phe180 a hydrophobic cleft for accommodating the B-ring. This cleft extends in a hydrophobic pocket (formed by Ile179, Leu173, and Tyr171) for binding the bromine atom, and Arg158 and Pro176 form a lid shielding this pocket from solvent. Superposition of the hSirt3/FdL-1/4′-bromo-resveratrol complex with a structure of hSirt3 in complex

Table 1. Data Collection and Refinement Statistics

	hSirt3/FdL-1/ 4′-Bromo-Resveratrol	hSirt3/ACS2/ 4′-Bromo-Resveratrol
Space group	R32	$P2_12_12$
Unit cell constants (Å)	a = b = 114.8, c = 123.7	a = 52.6, b = 159.7, c = 34.7
Resolution (Å)	46.1–2.1	46.1–2.0
Unique reflections	18,510	20,570
<I/σ> (outermost shell)	18.4 (2.8)	14.9 (2.8)
Completeness (outermost shell) (%)	100.0% (100.0)	99.6% (100.0)
R_{merge} (outermost shell) (%)[a]	8.5 (78.0)	5.9 (50.2)
R_{meas} (outermost shell) (%)[b]	9.1 (83.6)	6.8 (58.3)
Resolution range for refinement (Å)	46.1–2.1	46.1–2.0
Total number of reflections used	17,585	19,507
Number of atoms in asymmetric unit		
Protein	2,064	2,057
Ligands	95	79
Water	136	125
Rmsds		
Bond length (Å)	0.02	0.02
Bond angles (°)	2.2	1.9
Average B factor (Å2)		
Protein	38.5	39.9
Peptide	42.9	43.1
4′-bromo-resveratrol	66.5	68.5
Zinc ions	24.0	24.9
Final R_{cryst}/R_{free} (%)[c,d]	18.3/24.0	19.4/24.1

[a] $R_{merge} = \frac{\sum(I - \langle I \rangle)}{\sum I}$. I is the intensity of an individual measurement and $\langle I \rangle$ the corresponding mean value.

[b] $R_{meas} = \frac{\sum_h \sqrt{\frac{n_h}{n_h - 1}} \sum_i^{n_h} |\hat{I}_h - I_{h,i}|}{\sum_h \sum_i^{n_h} I_{h,i}}$ with $\hat{I}_h = \frac{1}{n_h} \sum_i^{n_h} I_{h,i}$.

[c] R-factor = $\frac{\sum ||F_{obs}| - k|F_{calc}||}{\sum |F_{obs}|}$; $|F_{obs}|$ is the observed and $|F_{calc}|$ the calculated structure factor amplitude.

[d] R_{free} was calculated from 5% of measured reflections omitted from refinement.

with ACS2 peptide and the NAD^+ analog carba-NAD^+ (Szczepankiewicz et al., 2012) reveals that 4′-bromo-resveratrol occupies part of the NAD^+ binding pocket, in particular the C-pocket (Figure 2E). This arrangement prevents the insertion of the NAD^+ nicotinamide moiety in the C-pocket necessary for catalysis, which indicates competitive inhibition with respect to this cosubstrate.

The overall hSirt3 and FdL1-peptide conformations in the superposition of the 4′-bromo-resveratrol complex with hSirt3 bound to FdL-1 and another resveratrol-related compound, piceatannol, are identical (Figure 2F), although the inhibition mechanisms of these compounds appear to be different. Piceatannol interacts extensively with the FdL-1 fluorophore, apparently causing nonproductive peptide binding (Gertz et al., 2012), while 4′-bromo-resveratrol does not directly contact this substrate peptide and blocks productive NAD^+ binding.

Crystal Structure of hSirt3 in Complex with ACS2 Substrate Peptide and 4′-Bromo-Resveratrol

Crystallizing hSirt3 in complex with ACS2 peptide, instead of FdL-1 peptide, in presence of 4′-bromo-resveratrol resulted in a different hSirt3/peptide/inhibitor arrangement. The compound molecule was found at the bottom of the Rossmann-fold domain, interacting with Arg139, Met331, and Arg335, rather than in the catalytic pocket (Figures 3A and 3B; Figure S2; Table 1). In this exposed position, the compound interacts only through its A-ring with this shallow hSirt3 pocket, and the bromo-containing aromatic ring points toward the symmetry-related monomer in the crystal lattice.

Superposition of the hSirt3/4′-bromo-resveratrol complexes with FdL-1 and ACS2 peptide, respectively, reveals that the inhibitor cannot bind at the catalytic pocket when the ACS2 peptide is bound, since it would clash with the C-terminal part of this substrate peptide (Figure 3C). The obtained hSirt3/ACS2/4′-bromo-resveratrol complex can either show a different compound site and mechanism for 4′-bromo-resveratrol inhibition than the FdL-1 complex, or this second site is a crystallization artifact and the inhibitory site simply not occupied due to competition with the highly concentrated ACS2 peptide. In fact, 4′-bromo-resveratrol in the complex structure with hSirt3/ACS2-peptide does not show many interactions with hSirt3, rendering it a less likely inhibition site. Figure 3D illustrates the hydrogen bonds of 4′-bromo-resveratrol with Arg139, Met331 (backbone), Arg335, and Arg384 of the symmetry-related monomer, and the very limited interaction interface with the hSirt3 monomer (see also Figure 3A).

To test whether the surface site occupied by 4′-bromo-resveratrol in its hSirt3/ACS2 complex is relevant for inhibition, the role of the interacting residues R139, M331, R335, and R384 were tested by site-directed mutagenesis to alanine. Microscale thermophoresis (MST) results indicated that the hSirt3-R335A variant might have a slightly reduced binding affinity for the compound compared to wild-type hSirt3 (Figure 3E), but the change was not statistically significant. The hSirt3 variants R384A, R139A, and M331A showed no change in the affinity for the compound. Moreover, we performed activity assays with 500 μM ACS2 as peptide substrate and in presence of 4′-bromo-resveratrol (at its IC_{50}, 140 μM) to examine the effects on the activity of the mutant proteins. The screening indicated that the activity of hSirt3-R335A is slightly higher than that for the other mutants and the wild-type protein (data not shown). An IC_{50} determination for 4′-bromo-resveratrol inhibition of hSirt3-R335A activity showed only a small shift of the inhibition curve compared to wild-type protein (Figure 3F), yielding IC_{50} values of 143.0 ± 3.6 (wild-type) and 179.2 ± 12.3 μM (hSirt3-R335A), respectively. Therefore, the position of 4′-bromo-resveratrol in the complex structure hSirt3-ACS2-4′-bromo-resveratrol appears to slightly influence activity but seems not to be primarily responsible for the inhibitory effect of the compound on hSirt3.

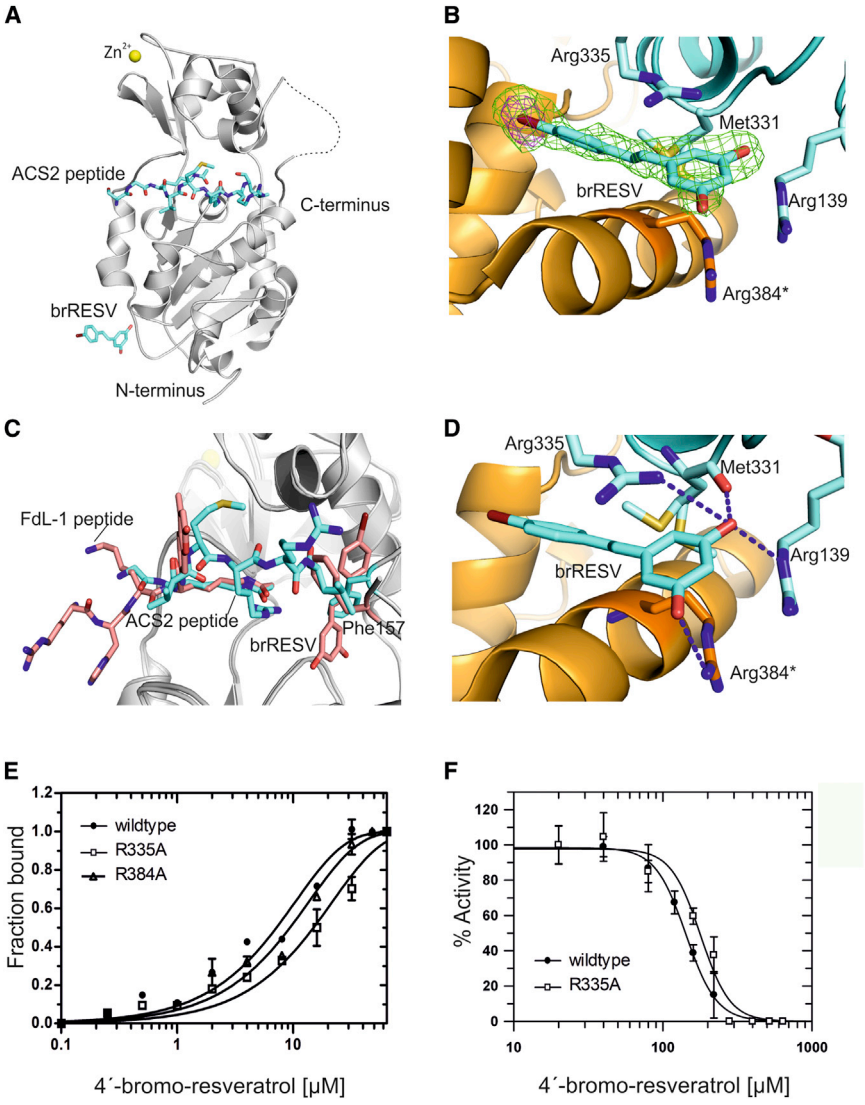

Figure 3. Crystal Structure of hSirt3 in Complex with ACS2 Substrate Peptide and Analysis of the Role of the Allosteric 4′-Bromo-Resveratrol Site

(A) Overall structure of hSirt3/ACS2/4′-bromo-resveratrol complex. A missing loop is indicated by a dashed line.

(B) 4′-bromo-resveratrol ligand of the hSirt3/ACS2/4′-bromo-resveratrol complex, overlaid with omit F_o-F_c difference density (2.5σ; green) and anomalous density (5σ; magenta) showing the position of Br and surrounding residues important for compound binding. Residues from the symmetry-related monomer are labeled with a star. See Figure S2 for $2F_o$-F_c density for peptide and inhibitor.

(C) Superposition of the hSirt3/ACS2/4′-bromo-resveratrol structure with the hSirt3/FdL-1/4′-bromo-resveratrol complex. FdL-1 peptide and 4′-bromo-resveratrol are shown in pink, ACS2 peptide in cyan. Phe157 of the hSirt3/ACS2/4′-bromo-resveratrol and hSirt3/FdL-1/4′-bromo-resveratrol complex are shown in cyan and pink, respectively.

(D) Closer view on the 4′-bromo-resveratrol binding site in the hSirt3/ACS2/4′-bromo-resveratrol complex showing interacting residues. Hydrogen bonds are indicated by dashed lines and residues of the next symmetry-related monomer are labeled with a star.

(E) Affinity measurements for binding of 4′-bromo-resveratrol to hSirt3 wild-type as well as R335A and R384A variants. Error bars: SD from two independent measurements.

(F) IC_{50} determination of 4′-bromo-resveratrol on wild-type hSirt3 or the R335A variant against 500 μM ACS2 peptide using MS. Error bars: SE of linear fits to time series experiments.

The 4′-Bromo-Resveratrol Inhibition Behavior Depends on the Peptide Substrate

The surface pocket accommodating 4′-bromo-resveratrol in the hSirt3/ACS2 complex would be allosteric and should act equally on different substrate peptides, while the internal 4′-bromo-resveratrol site of the complex with hSirt3/FdL-1 should lead to competition with ACS2 peptide, but not with the C-terminally shorter FdL-1 substrate. To analyze the relevance of the two identified 4′-bromo-resveratrol binding sites for inhibition, we therefore performed competition analyses.

To test for competition between 4'-bromo-resveratrol and FdL-1 peptide, IC_{50} values for 4′-bromo-resveratrol inhibition of hSirt3 were determined at three different concentrations of FdL-1 peptide (50, 100, and 200 μM). The IC_{50} values obtained were ~100 μM for all three peptide concentrations (Figure 4A), indicating that the inhibitor 4′-bromo-resveratrol does not compete against FdL-1.

To test for 4′-bromo-resveratrol competition with ACS2 peptide, MS assays were performed to determine K_m and V_{max} values for the peptide at different compound concentrations. The result shows that the higher the 4′-bromo-resveratrol concentration, the more the K_m for substrate peptide increases, or apparent affinity for substrate decreases, while the V_{max} is not altered, indicating competitive inhibition with respect to the peptide substrate (Figure 4B; Figure S3). This competition was confirmed through binding measurements. ACS2 peptide bound to apo hSirt3 with a K_d value of 64.4 ± 9.1 μM. In presence of 50 μM 4′-bromo-resveratrol, the K_d value increased to more than 200 μM (Figure 4C). Consistently, binding affinity of 4′-bromo-resveratrol to the apo protein was 7.6 ± 0.9 μM, and the K_d increased to higher than 37 μM in the presence of 500 μM ACS2 peptide (Figure 4D). Thus, 4′-bromo-resveratrol inhibits hSirt3 through competition with ACS2 peptide substrate. The K_i of 4′-bromo-resveratrol calculated from the IC_{50} based on peptide competition is ~8 μM, in good agreement with the measured binding affinity.

Our competition experiments with FdL-1 and ACS2 peptide indicate that hSirt3 inhibition is due to 4′-bromo-resveratrol binding to the internal site, which causes competition with the C-terminally longer ACS2 peptide and which would also lead to competition with NAD^+. We therefore also tested for

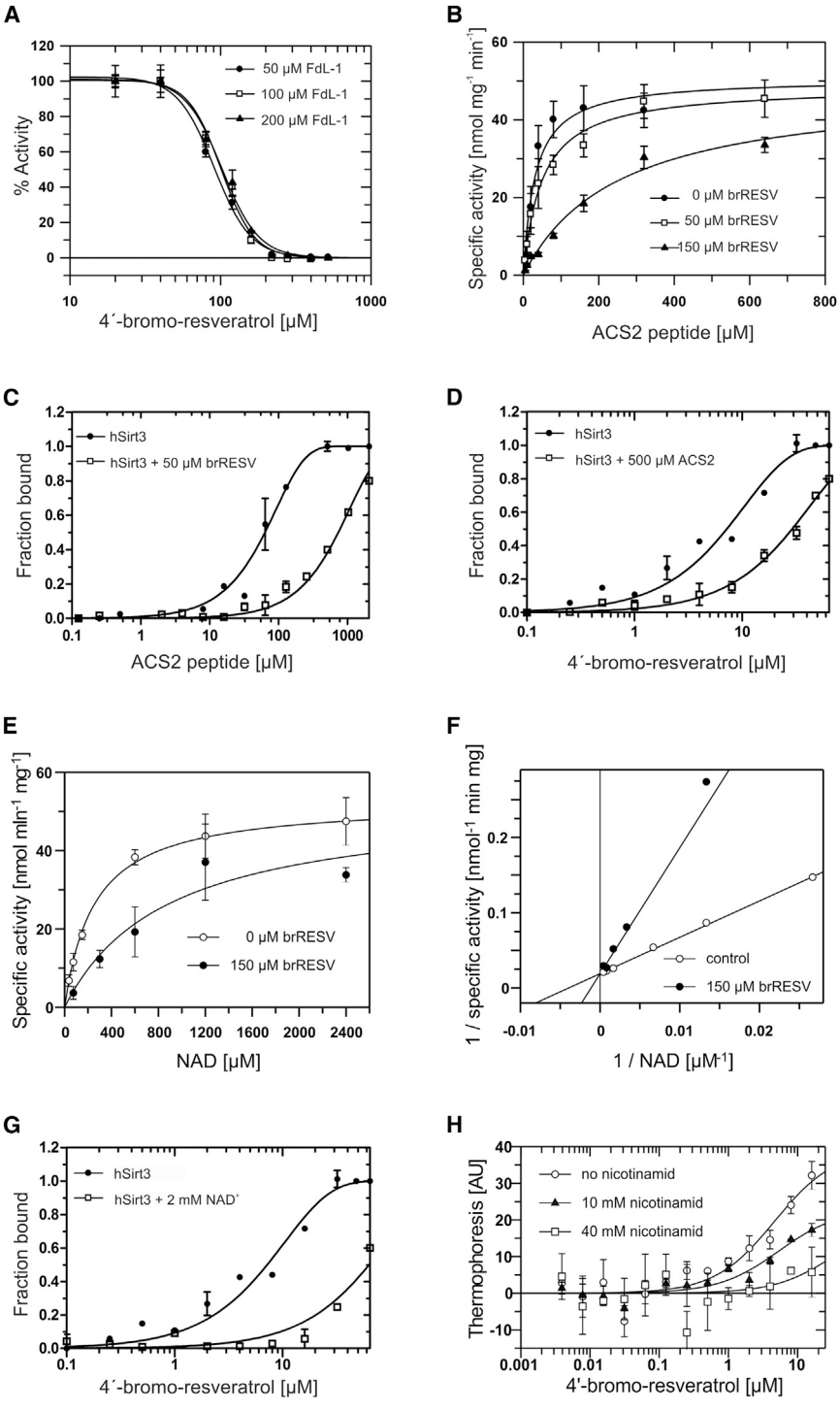

Figure 4. The 4′-Bromo-Resveratrol Inhibition Behavior Depends on the Peptide Substrate

(A) IC_{50} determination for 4′-bromo-resveratrol inhibition of hSirt3 at 50, 100, and 200 μM FdL-1 substrate peptide.

(B) 4′-Bromo-resveratrol inhibition of hSirt3 with ACS2 peptide as a substrate. 4′-Bromo-resveratrol concentrations of 0, 50, and 150 μM resulted in K_m values for substrate peptide of 31.3 ± 9.0, 48.6 ± 7.5, and 253.3 ± 52.9 μM, respectively, while the V_{max} is roughly constant at ~50 nmol mg^{-1} min^{-1}. Error bars: SE of linear fits to time series experiments. See Figure S3 for Lineweaver-Burk plots.

(C) Binding affinity of ACS2 peptide to hSirt3 in the presence or absence of 50 μM 4′-bromo-resveratrol.

(D) Binding affinity of 4′-bromo-resveratrol to hSirt3 in the presence or absence of 500 μM ACS2 peptide.

(E) 4′-bromo-resveratrol inhibition of hSirt3 activity against ACS2 peptide at varying NAD^+ concentrations. 4′-Bromo-resveratrol concentrations of 0 and 150 μM resulted in K_m values for the cosubstrate NAD^+ of 264.7 ± 53.4 and 753.6 ± 49.0, respectively, while the V_{max} is roughly constant at ~50 nmol mg^{-1} min^{-1}. Error bars: SE of linear fits to time series experiments.

(F) Lineweaver-Burk plot of the data for 4′-bromo-resveratrol inhibition of hSirt3 at varying NAD^+ concentrations shown in (E).

(G) Binding affinity of 4'-bromo-resveratrol to hSirt3 in the presence or absence of 2 mM NAD^+. The same data for apo hSirt3 as in (D) is included for comparison.

(H) Binding of 4′-bromo-resveratrol to hSirt3 in the presence or absence of 10 mM or 40 mM nicotinamide, respectively. Absolute values are plotted due to the lack of reliable upper baseline values for normalization.

(A, C, D, G, and H) Error bars: SD from two independent measurements.

competition between the cosubstrate and compound in hSirt3 binding and activity assays. Adding inhibitor to hSirt3 activity assays strongly increased the K_m for NAD^+ without affecting the V_{max} (Figures 4E and 4F), indicating competitive inhibition with respect to the cosubstrate. The binding affinity of 4′-bromo-resveratrol to the apo protein was 7.6 ± 0.9 μM, and the K_d increased to higher than 50 μM when measured in presence of 2 mM NAD^+ (Figure 4G), confirming competitive binding of inhibitor and cosubstrate. We further tested 4′-bromo-resveratrol binding in presence and absence of nicotinamide, which corresponds to the cosubstrate moiety that occupies the C-pocket of the NAD^+ binding site. This pocket also accommodates the A-ring of 4′-bromo-resveratrol in the internal site, and we indeed observed a weaker inhibitor affinity in presence of nicotinamide (Figure 4H) indicating competition for this site. These results show that 4′-bromo-resveratrol also competes with NAD^+, and in particular with its nicotinamide moiety, for binding to hSirt3, confirming that the internal 4′-bromo-resveratrol binding site is the one relevant for hSirt3 inhibition. Based on an NAD^+ competitive inhibition mechanism, the K_i for 4′-bromo-resveratrol calculated from the IC_{50} value is ~18 μM, in the range but slightly higher than expected from the compound's binding affinity.

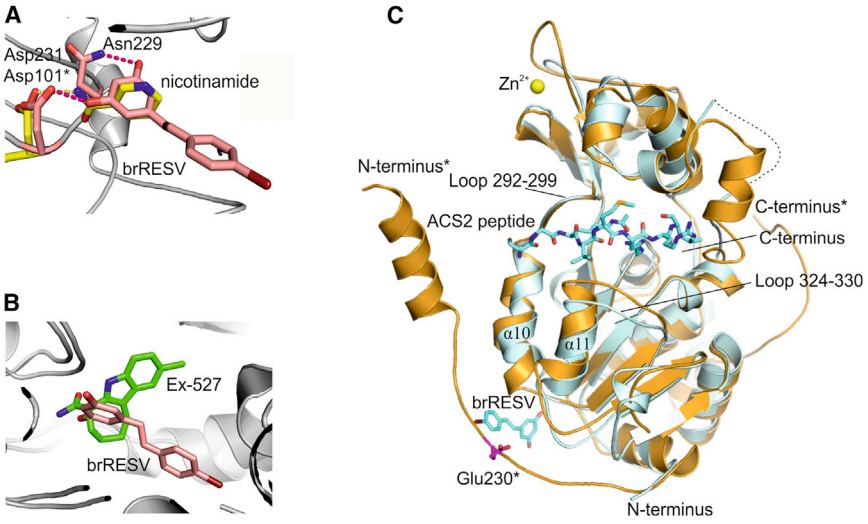

Figure 5. Analysis of the 4′-Bromo-Resveratrol Binding Sites through Comparison to other Sirtuin Structures

(A) Superposition of the hSirt3/FdL-1/4′-bromo-resveratrol complex with a Sir2Tm/p53/nicotinamide complex (PDB ID 1YC5; Avalos et al., 2005). Dashed lines indicate hydrogen bonds of the 4′-bromo-resveratrol A-ring hydroxyl groups and of the nicotinamide carboxamide group to protein residues. 4′-Bromo-resveratrol is shown in pink and nicotinamide in yellow. The protein part of the Sir2Tm/p53/nicotinamide complex is omitted for clarity. Sir2Tm residues are labeled with a star.

(B) Superposition of the hSirt3/FdL-1/4′-bromo-resveratrol complex with a hSirt1/NAD^+/Ex-527 complex (PDB ID 4I5I; Zhao, et al., 2013). 4′-Bromo-resveratrol (pink) and Ex-527 (green) both occupy the C site but extend in different directions.

(C) Superposition of the hSirt3/ACS2/4′-bromo-resveratrol complex (cyan) with a homology model of hSirt1 (orange). 4′-Bromo-resveratrol of hSirt3 is close to the putative position of Glu230 (magenta) of hSirt1 suggesting the involvement of the compound binding site to an allosteric hSirt1 activation mechanism. hSirt1 N and C termini and Glu230 are labeled with a star. A missing hSirt3 loop is indicated by a dashed line. See Figure S4C for a crystal contact blocking this site in the hSirt3/FdL-1/4′-bromo-resveratrol complex.

Our results show that the small change of one hydroxyl group of resveratrol to a bromine atom dramatically changes the effect on Sirtuins, and our structural data reveal the internal binding site exploited by this compound for potent Sirtuin inhibition.

DISCUSSION

Resveratrol was reported to activate hSirt1 and several of its orthologs (Howitz et al., 2003). Many studies on finding the activation mechanism failed (Moniot et al., 2012) and in particular, a hSirt1/resveratrol complex structure is lacking. Resveratrol also inhibits hSirt3, and we used the 4′-bromo reveratrol derivative to study its action on hSirt3. 4′-Bromo-resveratrol turned out to be a more potent hSirt3 inhibitor than resveratrol itself or its derivatives piceatannol and polydatin. A previous crystal structure of a hSirt3/FdL-1/piceatannol complex revealed an exposed binding site and a direct interaction between compound and FdL-1 fluorophore, which explained the influence of this fluorophore on compound effects (Borra et al., 2005; Gertz et al., 2012; Kaeberlein et al., 2005; Pacholec et al., 2010). However, the hSirt3/FdL-1/piceatannol complex would not easily explain the increased potency of a 4′-bromo derivative and the inhibition rather than activation of hSirt1, and we indeed find that 4′-bromo-resveratrol binds to a different site and does not contact the FdL-1 fluorophore. Binding of 4′-bromo-resveratrol to this ligand site (see below) is surprising considering the compound's very small structural difference to resveratrol and piceatannol. Our biochemical data confirm that 4′-bromo-resveratrol inhibits through binding to this internal site, and the compound thus defines an additional class of Sirtuin modulators, related to resveratrol in chemical structure but acting through a distinct-Sirtuin binding mode. Although 4′-bromo-resveratrol is an order of magnitude more potent than resveratrol (Gertz et al., 2012; Milne et al., 2007), potency and selectivity need to be improved either by modifying the compound or by identifying novel ligands for this site. Our structural data can support both approaches by providing a template for docking searches for new ligands and by suggesting modifications to 4′-bromo-resveratrol that might improve binding and selectivity. 4′-Bromo-resveratrol partially occupies the C pocket, where NAD^+ binds in its productive conformation with its nicotinamide moiety to initialize the reaction and where nicotinamide can bind to an alkylimidate complex (Sauve et al., 2006) for the reverse reaction (Figure 5A). A hydroxyl group of the 4′-bromo-resveratrol A-ring plays a role like the nicotinamide carboxamide group, which also interacts with the conserved Asp101 (Asp231 in hSirt3) in a Sir2Tm/nicotinamide complex (Avalos et al., 2005). The C-site is also exploited by Ex-527 (Gertz et al., 2013; Zhao et al., 2013), a potent hSirt1 inhibitor (Napper et al., 2005; Solomon et al., 2006). However, 4′-bromo-resveratrol and Ex-527 extend from the C-pocket in different directions (Figure 5B). While the kinked Ex-527 molecule extends perpendicular to its carbamide in a hydrophobic pocket close to the acetyl-Lys binding site, 4′-bromo-resveratrol extends with its B-ring toward a pocket close to the enzyme's surface. Similarily, the recently characterized hSirt3 binding modes of SRT1720 and of thieno[3,2-d]pyrimidine-6-carboxamides (Disch et al., 2013; Nguyen et al., 2013) show some overlap with 4′-bromo-resveratrol, but do not extend in the B-ring pocket (Figure S4A). The bromo-containing B-ring appears to show some rotational flexibility within this hydrophobic binding cleft, indicated by weak omit F_o-F_c density. However, the bromine anchors it through mainly hydrophobic interactions, explaining why 4′-bromo-resveratrol efficiently occupies this pocket for potent inhibition while the more polar resveratrol and piceatannol do not show significant affinity for this site. Adding a longer, hydrophilic group in meta position to the bromine for interaction with Glu198 might strengthen binding and thus increase potency. In Sirt5, the pocket entrance is tightened (Figure S4B) and more polar due to the Sirt5-specific Arg105 (Fischer et al., 2012), explaining Sirt5's insensitivity to 4′-bromo-resveratrol and suggesting that replacing the B-ring with a small polar group might enable to selectively target this

isoform. In hSirt1, the pocket is accessible but tightened compared to hSirt3 (Figure S4B), so that B-ring modifications should favor hSirt3 binding while B-ring replacements with smaller hydrophobic groups should lead to preferential hSirt1 binding. Our complex structure thus reveals a target site for Sirtuin inhibition, with 4′-bromo-resveratrol as a prototype inhibitor exploiting this pocket, and our results and analyses indicate potential and suggest strategies for using the compound and binding site as starting points for the development of improved Sirtuin inhibitors.

4′-Bromo-resveratrol shows the same inhibitory effect on hSirt1 as on hSirt3, and a similar internal binding pocket is present in hSirt1 (see above), strongly suggesting that hSirt1 inhibition is based on the same binding site and competitive mechanism. Interestingly, this competition excludes the inhibitory 4′-bromo-resveratrol site as the binding pocket for the almost identical, hSirt1 activating compound resveratrol, which constitutes a remarkable switch in binding sites through a very small difference in compound structure. The weak 4′-bromo-resveratrol interaction site at the bottom of the Rossmann-fold domain (its affinity has to be equal to or lower than the compound affinity measured under ACS2 peptide saturation, $K_d \geq 37\ \mu M$), however, might hint at an allosteric hSirt1 site for resveratrol binding. A hSirt1 model, based on its catalytic domain structure (Zhao et al., 2013) and an N-terminally longer hSirt2 structure (Moniot et al., 2013), indicates an extended conformation for an N-terminal extension (residues 210–240) implicated in activation (Milne et al., 2007; Figure 5C), consistent with H/D exchange data (Hubbard et al., 2013). Superposition with hSirt3/ACS2/4′-bromo-resveratrol indicates that the extension could contribute to the external 4′-bromo-resveratrol binding site. In particular, hSirt1-Glu230, a residue essential for activation (Hubbard et al., 2013), is located next to this binding site (Figure 5C), and we thus speculate that it might serve as allosteric activation site in hSirt1. It is connected to substrate binding loops (324–330 and 292–299, hSirt3 numbering) through α11 and α10 (Figure 5C), and a coupling of these sites would provide a molecular activation model explaining the substrate sequence influence on compound effects (Lakshminarasimhan et al., 2013a). A recent yeast Sir2 structure (Hsu et al., 2013) revealed binding of the activator protein Sir4 between α10/11 and an N-terminal regulatory domain of Sir2 positioned similar to the Sirt1 extension, supporting such an allosteric activation mechanism, but definite conclusions on the mechanism of hSirt1 activation will require further studies on this protein. A superposition of hSirt3/ACS2/4′-bromo-resveratrol and hSirt3/FdL-1/4′-bromo-resveratrol reveals that in the FdL-1 complex, a loop of a symmetry-related monomer prevents binding to this allosteric site (Figure S4C). This difference in crystal packing explains why this site was not occupied in our FdL-1 complex structure in addition to the internal binding site responsible for potent hSirt1/3 inhibition.

SIGNIFICANCE

Sirtuins have been implicated in aging-related diseases and are considered attractive drug targets. Extensive research efforts aim to identify potent and specific Sirtuin inhibitor for in vivo studies and therapy. Human Sirt1 and its orthologs can also be activated by small molecules such as resveratrol, and the resulting beneficial health effects have spurred research on Sirtuin activators. The development of improved Sirtuin inhibitors and activators has been hampered, however, by the lack of knowledge on binding sites and modulation mechanisms of available compounds. We studied Sirtuin modulation by using 4′-bromo-resveratrol, a derivative of the weak Sirt1 activator and weak Sirt3 inhibitor resveratrol that can be identified unequivocally in crystal structures. The compound inhibited Sirt3 with much higher potency than resveratrol, and it also inhibited rather than activated Sirt1. Crystal structures of human Sirt3/peptide complexes in presence of 4′-bromo-resveratrol identified two compound binding sites. An internal site, overlapping with the active site, causes the potent inhibitory effect. The compound interferes with NAD^+ and substrate peptide binding, and it extends its bromo-phenyl group in a so far not recognized hydrophobic active site pocket. These results identify a different type of Sirtuin inhibitor and an additional Sirtuin site that can be targeted for inhibitor development. The second binding site for 4′-bromo-resveratrol is located on the surface of Sirt3 and connected through two helices to peptide-binding active site loops. In Sirt1, this site appears to comprise a residue that is essential for its activation by small molecules and it therefore constitutes a candidate for the long-sought allosteric Sirt1 activator binding site. Our study thus provides insights into binding sites and mechanisms for Sirtuin regulation, supporting the development of improved Sirtuin-targeting drugs.

EXPERIMENTAL PROCEDURES

Chemicals and Peptides

Chemicals were from Sigma if not stated otherwise. 5-(2-(4-hydroxyphenyl)vinyl)-1,3-benzenediol was from Matrix Scientific. ACS2 peptide (TRSGacetylKVMRRL) was synthesized and HPLC purified by GL Biochem, FdL-1 peptide was from Enzo Life Sciences.

Cloning, Protein Expression, and Purification

hSirt1, hSirt3, and hSirt5 were cloned, expressed, and purified as described in previous reports (Gertz et al., 2012; Lakshminarasimhan et al., 2013b). Briefly, full-length hSirt1 (in vector pET15b coding for an N-terminal His-tag; Life Technologies) and the catalytic core domains of hSirt3 (residues 118–399, in vector pVFT3S [Sungkyunkwan University, South Korea] coding for an N-terminal His-Trx-tag) and hSirt5 (residues 34–302 in vector pET151/D-TOPO coding an N-terminal His-tag) were expressed in *Escherichia coli* strain BL21DE3 Rosetta2 (Merck, Whitehouse Station, NJ) at 15°C upon induction with 0.5 mM isopropyl-β-D-thiogalactoside. The fusion proteins were purified by affinity chromatography with talon resin. The His-Trx-tag of hSirt3 was removed by addition of Tobacco Etch Virus (TEV) protease. The tag-cleaved hSirt3 was resubjected to talon chromatography to remove tag and protease. Finally, hSirt1, hSirt3, and hSirt5 were subjected to Superose-12 gel filtration chromatography (GE Healthcare), and the purified proteins were shock-frozen and stored at −80°C.

Crystallization and Structure Solution

hSirt3 (8 mg/ml in 20 mM Tris/HCl, pH 7.8, and 150 mM NaCl) was crystallized in complex with FdL-1 or ACS2 peptide and 4′-bromo-resveratrol after pre-incubation with 2 mM peptide and 1 mM compound (10% [v/v] DMSO) for 1 hr on ice. Protein solution was mixed with reservoir (hSirt3/FdL-1/4′-bromo-resveratrol, 200 mM NaCl, 100 mM HEPES pH 7, 10% [v/v] isopropanol; hSirt3/ACS2/4′-bromo-resveratrol, 250 mM $[NH_4]_2SO_4$, 100 mM BisTris pH 6, 21% [w/v] PEG 3350) in a 1:1 ratio and equilibrated against 0.4 ml reservoir at 20°C. The crystals were transferred to cryo solution containing reservoir,

25% (v/v) glycerol, peptide, and 4′-bromo-resveratrol and frozen in liquid nitrogen.

The X-ray diffraction data were collected at 100 K with an MX-225 CCD detector (Rayonix) at beam line MX14.1 of the BESSY II electron storage ring (Mueller et al., 2012). The wavelength was 0.92 Å, allowing observation of the anomalous diffraction of the Br atom. Diffraction data were processed using XDS (Kabsch, 2010). Crystal structures were solved by Patterson searches with the program MolRep (Vagin and Isupov, 2001) using the protein part of the hSirt3/FdL-1/PCT complex (Protein Data Bank [PDB] ID 4HD8; Gertz et al., 2012) as a search model. Structure refinement was performed using Refmac (Murshudov et al., 1997), and manual rebuilding was done in Coot (Emsley and Cowtan, 2004). Parameter files for 4′-bromo-resveratrol were generated using ProDrg (Schüttelkopf and van Aalten, 2004). The quality of the refined structures was evaluated by using Coot and MolProbity (Chen et al., 2010).

The FdL-1 fluorophore in the complex hSirt3/FdL-1/4′-bromo-resveratrol was modeled as the commonly used 7-amino-4-methylcoumarin ring (Gertz et al., 2012). A small blob of additional electron density at the methyl group of the fluorophore might indicate that a slightly different group is attached to the coumarin, and we indeed find a difference (~43 Da) between calculated and measured FdL-1 mass (data not shown). However, no fluorophore details are available from the manufacturer (Enzo Life Sciences), and the mass difference would also be explained by the common acetylation of the peptide's N terminus. We therefore kept the 7-amino-4-methylcoumarin as fluorophore in our FdL-1 model.

Homology Modeling of N-Terminally Extended hSirt1

A homology model for hSirt1 (UniProt entry Q96EB6) residues 210–516 was generated using the published hSirt1 catalytic core crystal structure (residues 241–516; PDB ID 4I5I; Zhao et al., 2013) and a re-refined crystal structure of hSirt2 residues 34–356 (PDB ID 3ZGO; Moniot et al., 2013) as templates. A structure-based alignment of the template sequences was generated with STRAP (Gille and Frömmel, 2001) and the extended hSirt1 sequence added manually. The hSirt1 model was generated from this alignment by using Modeler version 9.10 (Šali and Blundell, 1993).

Deacetylation Assays

The deacylase activities of hSirt1, hSirt3, and hSirt5 were tested using a commercial Fluor-de-lys assay kit (Enzo Life Sciences) containing acetylated (hSirt1, hSirt3) or succinylated (hSirt5) FdL-substrate peptides with a C-terminally attached fluorophore. One microgram of hSirt1 was incubated with 25 μM FdL-1 and 50 μM NAD^+, 1.5 μg hSirt3 with 0.1 mM FdL-1 and 2.5 mM NAD^+, or 0.5 μg hSirt5 with 0.1 mM FdL-Succinyl Green and 2.5 mM NAD^+ in the presence of 0.2 mM or 1 mM compound and 2% (v/v) DMSO, or with 2% (v/v) DMSO without compound as a control, for 30 min at 37°C. The mixture was then incubated with the trypsin developer for 45 min at room temperature to release the fluorophore from deacetylated FdL-1. Fluorescence was determined at excitation wavelengths of 360 nm (acetyl-FdL-1) and 486 nm (FdL-Succinyl Green), respectively, and emission wavelengths of 460 nm (acetyl-FdL-1) and 530 nm (FdL-Succinyl Green).

For the MS assay, 10 μM hSirt3 was incubated with 0.5 mM ACS2 peptide and 2.5 mM NAD^+ (or the indicated concentrations in titration experiments) in the presence or absence of different 4′-bromo-resveratrol concentrations in 2% (v/v) DMSO, or with 2% (v/v) DMSO without compound as a control, at 37°C. The reaction was stopped after different time points by adding 0.25% (v/v) trifluoroacetic acid followed by dilution to 1 μM peptide in 0.1% (v/v) formic acid. Finally, the solution was filtered to separate ACS2 peptide from the reaction mixture and subjected to nano-LC-MS/MS analysis as described previously (Fischer et al., 2012). Specific deacetylation activity was determined by linear fitting of the time-series experiments.

Binding Analysis by Microscale Thermophoresis

Binding affinities were measured by microscale thermophoresis (Wienken et al., 2010) with 1 μM hSirt3 in 20 mM Tris pH 7.8, and 150 mM NaCl in the presence or absence of competitor and the indicated 4′-bromo-resveratrol or ACS2 peptide concentrations. Protein and ligands were mixed and transferred into glass capillaries at room temperature, and thermophoresis was analyzed at 25°C using a NanoTemper Monolith NT.label-free instrument (NanoTemper Technologies, München, Germany) and the intrinsic protein fluorescence signal (excitation at 280 nm, emission at 360 nm). The excitation LED power was set to 25%, and the IR-laser power to 20%–80%. Affinities were determined through non-linear fitting (1-site equation) of the measured thermophoresis values using Prism (GraphPad Software, La Jolla, CA), and signals are presented normalized to the signal difference between baselines if saturation could be reached. Each experiment was repeated at least twice.

Statistical Analysis

Error bars for the MS activity assay represent SEs of linear regression analysis of time series experiments with four data points. For FdL activity data and binding measurements, error bars represent SDs from two independent measurements.

ACCESSION NUMBERS

The PDB accession numbers for the coordinates and structure factors for the crystal structures of hSirt3 in complex with peptide and 5-(2-(4-bromophenyl) vinyl)-1,3-benzenediol are 4C7B (FdL-1 peptide complex) and 4C78 (ACS2 peptide complex).

SUPPLEMENTAL INFORMATION

Supplemental Information includes four figures and can be found with this article online at http://dx.doi.org/10.1016/j.chembiol.2013.09.019.

ACKNOWLEDGMENTS

We thank Norbert Grillenbeck, Dr. Sebastien Moniot, Dr. Michael Weyand, and the beamline staff of BESSY MX14.1 (Helmholtz-Zentrum Berlin) for technical assistance. This work was supported through grant STE1701/5 of Deutsche Forschungsgemeinschaft (to C.S.) and Elite Network Bavaria (to G.N. and C.S.).

Received: March 21, 2013
Revised: September 11, 2013
Accepted: September 13, 2013
Published: November 7, 2013

REFERENCES

Avalos, J.L., Bever, K.M., and Wolberger, C. (2005). Mechanism of sirtuin inhibition by nicotinamide: altering the NAD(+) cosubstrate specificity of a Sir2 enzyme. Mol. Cell *17*, 855–868.

Borra, M.T., Langer, M.R., Slama, J.T., and Denu, J.M. (2004). Substrate specificity and kinetic mechanism of the Sir2 family of NAD+-dependent histone/protein deacetylases. Biochemistry *43*, 9877–9887.

Borra, M.T., Smith, B.C., and Denu, J.M. (2005). Mechanism of human SIRT1 activation by resveratrol. J. Biol. Chem. *280*, 17187–17195.

Chen, L. (2011). Medicinal chemistry of sirtuin inhibitors. Curr. Med. Chem. *18*, 1936–1946.

Chen, V.B., Arendall, W.B., 3rd, Headd, J.J., Keedy, D.A., Immormino, R.M., Kapral, G.J., Murray, L.W., Richardson, J.S., and Richardson, D.C. (2010). MolProbity: all-atom structure validation for macromolecular crystallography. Acta Crystallogr. D Biol. Crystallogr. *66*, 12–21.

Cohen, H.Y., Miller, C., Bitterman, K.J., Wall, N.R., Hekking, B., Kessler, B., Howitz, K.T., Gorospe, M., de Cabo, R., and Sinclair, D.A. (2004). Calorie restriction promotes mammalian cell survival by inducing the SIRT1 deacetylase. Science *305*, 390–392.

Disch, J.S., Evindar, G., Chiu, C.H., Blum, C.A., Dai, H., Jin, L., Schuman, E., Lind, K.E., Belyanskaya, S.L., Deng, J., et al. (2013). Discovery of thieno[3,2-d]pyrimidine-6-carboxamides as potent inhibitors of SIRT1, SIRT2, and SIRT3. J. Med. Chem. *56*, 3666–3679.

Du, J., Zhou, Y., Su, X., Yu, J.J., Khan, S., Jiang, H., Kim, J., Woo, J., Kim, J.H., Choi, B.H., et al. (2011). Sirt5 is a NAD-dependent protein lysine demalonylase and desuccinylase. Science *334*, 806–809.

Emsley, P., and Cowtan, K. (2004). Coot: model-building tools for molecular graphics. Acta Crystallogr. D Biol. Crystallogr. *60*, 2126–2132.

Fischer, F., Gertz, M., Suenkel, B., Lakshminarasimhan, M., Schutkowski, M., and Steegborn, C. (2012). Sirt5 deacylation activities show differential sensitivities to nicotinamide inhibition. PLoS ONE *7*, e45098.

Frye, R.A. (2000). Phylogenetic classification of prokaryotic and eukaryotic Sir2-like proteins. Biochem. Biophys. Res. Commun. *273*, 793–798.

Gertz, M., and Steegborn, C. (2010). Function and regulation of the mitochondrial sirtuin isoform Sirt5 in Mammalia. Biochim. Biophys. Acta *1804*, 1658–1665.

Gertz, M., Nguyen, G.T., Fischer, F., Suenkel, B., Schlicker, C., Fränzel, B., Tomaschewski, J., Aladini, F., Becker, C., Wolters, D., and Steegborn, C. (2012). A molecular mechanism for direct sirtuin activation by resveratrol. PLoS ONE *7*, e49761.

Gertz, M., Fischer, F., Nguyen, G.T.T., Lakshminarasimhan, M., Schutkowski, M., Weyand, M., and Steegborn, C. (2013). Ex-527 inhibits Sirtuins by exploiting their unique NAD+-dependent deacetylation mechanism. Proc. Natl. Acad. Sci. USA *110*, E2772–E2781.

Gille, C., and Frömmel, C. (2001). STRAP: editor for STRuctural Alignments of Proteins. Bioinformatics *17*, 377–378.

Guarente, L. (2005). Calorie restriction and SIR2 genes—towards a mechanism. Mech. Ageing Dev. *126*, 923–928.

Guarente, L., and Picard, F. (2005). Calorie restriction—the SIR2 connection. Cell *120*, 473–482.

Haigis, M.C., and Sinclair, D.A. (2010). Mammalian sirtuins: biological insights and disease relevance. Annu. Rev. Pathol. *5*, 253–295.

Haigis, M.C., Mostoslavsky, R., Haigis, K.M., Fahie, K., Christodoulou, D.C., Murphy, A.J., Valenzuela, D.M., Yancopoulos, G.D., Karow, M., Blander, G., et al. (2006). SIRT4 inhibits glutamate dehydrogenase and opposes the effects of calorie restriction in pancreatic beta cells. Cell *126*, 941–954.

Hebert, A.S., Dittenhafer-Reed, K.E., Yu, W., Bailey, D.J., Selen, E.S., Boersma, M.D., Carson, J.J., Tonelli, M., Balloon, A.J., Higbee, A.J., et al. (2013). Calorie restriction and SIRT3 trigger global reprogramming of the mitochondrial protein acetylome. Mol. Cell *49*, 186–199.

Hoff, K.G., Avalos, J.L., Sens, K., and Wolberger, C. (2006). Insights into the sirtuin mechanism from ternary complexes containing NAD+ and acetylated peptide. Structure *14*, 1231–1240.

Howitz, K.T., Bitterman, K.J., Cohen, H.Y., Lamming, D.W., Lavu, S., Wood, J.G., Zipkin, R.E., Chung, P., Kisielewski, A., Zhang, L.L., et al. (2003). Small molecule activators of sirtuins extend Saccharomyces cerevisiae lifespan. Nature *425*, 191–196.

Hsu, H.C., Wang, C.L., Wang, M., Yang, N., Chen, Z., Sternglanz, R., and Xu, R.M. (2013). Structural basis for allosteric stimulation of Sir2 activity by Sir4 binding. Genes Dev. *27*, 64–73.

Hubbard, B.P., Gomes, A.P., Dai, H., Li, J., Case, A.W., Considine, T., Riera, T.V., Lee, J.E., e, S.Y., Lamming, D.W., et al. (2013). Evidence for a common mechanism of SIRT1 regulation by allosteric activators. Science *339*, 1216–1219.

Jin, L., Wei, W., Jiang, Y., Peng, H., Cai, J., Mao, C., Dai, H., Choy, W., Bemis, J.E., Jirousek, M.R., et al. (2009). Crystal structures of human SIRT3 displaying substrate-induced conformational changes. J. Biol. Chem. *284*, 24394–24405.

Kabsch, W. (2010). Xds. Acta Crystallogr. D Biol. Crystallogr. *66*, 125–132.

Kaeberlein, M., McDonagh, T., Heltweg, B., Hixon, J., Westman, E.A., Caldwell, S.D., Napper, A., Curtis, R., DiStefano, P.S., Fields, S., et al. (2005). Substrate-specific activation of sirtuins by resveratrol. J. Biol. Chem. *280*, 17038–17045.

Lakshminarasimhan, M., Rauth, D., Schutkowski, M., and Steegborn, C. (2013a). Sirt1 activation by resveratrol is substrate sequence-selective. Aging (Albany, N.Y. Online) *5*, 151–154.

Lakshminarasimhan, M., Curth, U., Moniot, S., Mosalaganti, S., Raunser, S., and Steegborn, C. (2013b). Molecular architecture of the human protein deacetylase Sirt1 and its regulation by AROS and resveratrol. Biosci. Rep. *33*, e00037.

Laurent, G., German, N.J., Saha, A.K., de Boer, V.C., Davies, M., Koves, T.R., Dephoure, N., Fischer, F., Boanca, G., Vaitheesvaran, B., et al. (2013). SIRT4 coordinates the balance between lipid synthesis and catabolism by repressing malonyl CoA decarboxylase. Mol. Cell *50*, 686–698.

Michan, S., and Sinclair, D. (2007). Sirtuins in mammals: insights into their biological function. Biochem. J. *404*, 1–13.

Milne, J.C., Lambert, P.D., Schenk, S., Carney, D.P., Smith, J.J., Gagne, D.J., Jin, L., Boss, O., Perni, R.B., Vu, C.B., et al. (2007). Small molecule activators of SIRT1 as therapeutics for the treatment of type 2 diabetes. Nature *450*, 712–716.

Moniot, S., Weyand, M., and Steegborn, C. (2012). Structures, substrates, and regulators of Mammalian sirtuins - opportunities and challenges for drug development. Front Pharmacol *3*, 16.

Moniot, S., Schutkowski, M., and Steegborn, C. (2013). Crystal structure analysis of human Sirt2 and its ADP-ribose complex. J. Struct. Biol. *182*, 136–143.

Mueller, U., Darowski, N., Fuchs, M.R., Förster, R., Hellmig, M., Paithankar, K.S., Pühringer, S., Steffien, M., Zocher, G., and Weiss, M.S. (2012). Facilities for macromolecular crystallography at the Helmholtz-Zentrum Berlin. J. Synchrotron Radiat. *19*, 442–449.

Murshudov, G.N., Vagin, A.A., and Dodson, E.J. (1997). Refinement of macromolecular structures by the maximum-likelihood method. Acta Crystallogr. D Biol. Crystallogr. *53*, 240–255.

Nakagawa, T., Lomb, D.J., Haigis, M.C., and Guarente, L. (2009). SIRT5 Deacetylates carbamoyl phosphate synthetase 1 and regulates the urea cycle. Cell *137*, 560–570.

Napper, A.D., Hixon, J., McDonagh, T., Keavey, K., Pons, J.F., Barker, J., Yau, W.T., Amouzegh, P., Flegg, A., Hamelin, E., et al. (2005). Discovery of indoles as potent and selective inhibitors of the deacetylase SIRT1. J. Med. Chem. *48*, 8045–8054.

Newman, J.C., He, W., and Verdin, E. (2012). Mitochondrial protein acylation and intermediary metabolism: regulation by sirtuins and implications for metabolic disease. J. Biol. Chem. *287*, 42436–42443.

Nguyen, G.T., Schaefer, S., Gertz, M., Weyand, M., and Steegborn, C. (2013). Structures of human sirtuin 3 complexes with ADP-ribose and with carba-NAD+ and SRT1720: binding details and inhibition mechanism. Acta Crystallogr. D Biol. Crystallogr. *69*, 1423–1432.

North, B.J., Marshall, B.L., Borra, M.T., Denu, J.M., and Verdin, E. (2003). The human Sir2 ortholog, SIRT2, is an NAD+-dependent tubulin deacetylase. Mol. Cell *11*, 437–444.

Pacholec, M., Bleasdale, J.E., Chrunyk, B., Cunningham, D., Flynn, D., Garofalo, R.S., Griffith, D., Griffor, M., Loulakis, P., Pabst, B., et al. (2010). SRT1720, SRT2183, SRT1460, and resveratrol are not direct activators of SIRT1. J. Biol. Chem. *285*, 8340–8351.

Park, S.-J., Ahmad, F., Philp, A., Baar, K., Williams, T., Luo, H., Ke, H., Rehmann, H., Taussig, R., Brown, A.L., et al. (2012). Resveratrol ameliorates aging-related metabolic phenotypes by inhibiting cAMP phosphodiesterases. Cell *148*, 421–433.

Pirola, L., and Fröjdö, S. (2008). Resveratrol: one molecule, many targets. IUBMB Life *60*, 323–332.

Rahman, S., and Islam, R. (2011). Mammalian Sirt1: insights on its biological functions. Cell Commun. Signal. *9*, 11.

Šali, A., and Blundell, T.L. (1993). Comparative protein modelling by satisfaction of spatial restraints. J. Mol. Biol. *234*, 779–815.

Sanders, B.D., Jackson, B., and Marmorstein, R. (2010). Structural basis for sirtuin function: what we know and what we don't. Biochim. Biophys. Acta *1804*, 1604–1616.

Sauve, A.A., and Youn, D.Y. (2012). Sirtuins: NAD(+)-dependent deacetylase mechanism and regulation. Curr. Opin. Chem. Biol. *16*, 535–543.

Sauve, A.A., Wolberger, C., Schramm, V.L., and Boeke, J.D. (2006). The biochemistry of sirtuins. Annu. Rev. Biochem. *75*, 435–465.

Schüttelkopf, A.W., and van Aalten, D.M. (2004). PRODRG: a tool for high-throughput crystallography of protein-ligand complexes. Acta Crystallogr. D Biol. Crystallogr. *60*, 1355–1363.

Solomon, J.M., Pasupuleti, R., Xu, L., McDonagh, T., Curtis, R., DiStefano, P.S., and Huber, L.J. (2006). Inhibition of SIRT1 catalytic activity increases

p53 acetylation but does not alter cell survival following DNA damage. Mol. Cell. Biol. *26*, 28–38.

Szczepankiewicz, B.G., Dai, H., Koppetsch, K.J., Qian, D., Jiang, F., Mao, C., and Perni, R.B. (2012). Synthesis of carba-NAD and the structures of its ternary complexes with SIRT3 and SIRT5. J. Org. Chem. *77*, 7319–7329.

Vagin, A.A., and Isupov, M.N. (2001). Spherically averaged phased translation function and its application to the search for molecules and fragments in electron-density maps. Acta Crystallogr. D Biol. Crystallogr. *57*, 1451–1456.

Verdin, E., Hirschey, M.D., Finley, L.W.S., and Haigis, M.C. (2010). Sirtuin regulation of mitochondria: energy production, apoptosis, and signaling. Trends Biochem. Sci. *35*, 669–675.

Villalba, J.M., and Alcaín, F.J. (2012). Sirtuin activators and inhibitors. Biofactors *38*, 349–359.

Wienken, C.J., Baaske, P., Rothbauer, U., Braun, D., and Duhr, S. (2010). Protein-binding assays in biological liquids using microscale thermophoresis. Nat Commun *1*, 100.

Zhao, X., Allison, D., Condon, B., Zhang, F., Gheyi, T., Zhang, A., Ashok, S., Russell, M., Macewan, I., Qian, Y., et al. (2013). The 2.5 A crystal structure of the SIRT1 catalytic domain bound to nicotinamide adenine dinucleotide (NAD+) and an indole (EX527 analog) reveals a novel mechanism of histone deacetylase inhibition. J. Med. Chem. *56*, 761–780.